



TITLE:

Impacts of ocean wave - dependent momentum flux on global ocean climate

AUTHOR(S):

Shimura, Tomoya; Hemer, Mark; Lenton, Andrew;
Chamberlain, Matthew A.; Monselesan, Didier

CITATION:

Shimura, Tomoya ...[et al]. Impacts of ocean wave - dependent momentum flux on global ocean climate. *Geophysical Research Letters* 2020, 47(20): e2020GL089296.

ISSUE DATE:

2020-10-28

URL:

<http://hdl.handle.net/2433/261801>

RIGHT:

An edited version of this paper was published by AGU. Copyright 2020 American Geophysical Union.; The full-text file will be made open to the public on 22 April 2021 in accordance with publisher's 'Terms and Conditions for Self-Archiving'.

Geophysical Research Letters

RESEARCH LETTER

10.1029/2020GL089296

Key Points:

- Wave-dependent momentum fluxes are implemented in a global ocean-sea ice model
- This results in a significantly improved ability to reproduce observed ocean climate state and variability
- Accounting for wave-dependent momentum fluxes significantly improves the simulation of ocean heat content

Supporting Information:

- Supporting Information S1

Correspondence to:

T. Shimura,
shimura.tomoya.2v@kyoto-u.ac.jp

Citation:

Shimura, T., Hemer, M., Lenton, A., Chamberlain, M. A., & Monselesan, D. (2020). Impacts of ocean wave-dependent momentum flux on global ocean climate. *Geophysical Research Letters*, 47, e2020GL089296. <https://doi.org/10.1029/2020GL089296>

Received 25 JUN 2020

Accepted 12 OCT 2020

Accepted article online 14 OCT 2020

Impacts of Ocean Wave-Dependent Momentum Flux on Global Ocean Climate

Tomoya Shimura¹ , Mark Hemer² , Andrew Lenton^{2,3,4} , Matthew A. Chamberlain² , and Didier Monselesan² 

¹Disaster Prevention Research Institute, Kyoto University, Uji, Kyoto, Japan, ²CSIRO Oceans and Atmosphere, Hobart, Tasmania, Australia, ³Centre for Southern Hemisphere Research, Hobart, Tasmania, Australia, ⁴Australian Antarctic Partnership Program, IMAS, UTas, Hobart, Tasmania, Australia

Abstract Accurate knowledge of air-sea fluxes of momentum, heat, and carbon are central to fully understanding the evolution of the climate system. The role of ocean surface waves has been largely overlooked in global climate models despite the growing body of work elucidating the influence of ocean wave state on air-sea fluxes. Here we account for the impact of ocean surface waves on global ocean climate using a global ocean model through implementation of wave-dependent momentum fluxes. Wave-dependent momentum fluxes improve the simulation of observed ocean heat content (OHC) through increasing the trend in OHC over the last three decades. Specifically, the larger increase in OHC is attributable to increased net heat flux in the Southern Hemisphere (SH). These results highlight the important role of accounting for wave-dependent momentum transfer in terms of both simulating future climate and understanding changes over the recent historical period.

Plain Language Summary Climate change is one of the main issues of sustainable development. The projection of climate change is important for assessment of impact on our environment, and the global climate model is used for the climate change projection. Accurate knowledge of momentum, heat, and carbon transfer at the atmosphere-ocean interface, so-called air-sea fluxes, is central to fully understanding the evolution of the climate system. Ocean surface waves exist everywhere in the global atmosphere-ocean interface. Many previous studies found that the air-sea fluxes are controlled by ocean surface waves. However, the roles of ocean surface waves are ignored in the global climate model. Here we account for the impact of ocean surface waves on global ocean climate. Ocean wave-dependent fluxes improve the simulation of ocean heat storage through increasing the trend in ocean heat storage over the last three decades to be more in line with observed historical changes. These results highlight the important role of accounting for wave-dependent air-sea fluxes in terms of both simulating future climate and understanding changes over the recent historical period.

1. Introduction

Global warming is now evident and both historical and future climate change must be accurately determined to guide future mitigation and adaptation efforts. Anthropogenic climate change is driven by a radiation imbalance between incoming solar radiation and outgoing thermal radiation at the top of the atmosphere that results from increased concentration of greenhouse gases. In addition to this imbalance at the top of atmosphere, heat flux imbalance at the atmosphere-ocean (and atmosphere-land) interface determines the global atmospheric temperature change.

The rate of global warming is mediated by the uptake of heat and carbon by the ocean (Meehl et al., 2011). The evidence for ocean warming due to increased ocean heat uptake (heat flux to ocean) is compelling (Balmaseda et al., 2013; Rhein et al., 2013; Roemmich et al., 2015). However, in terms of heat, this comes at the price of thermosteric sea level rise (Levitus et al., 2012). In the 2000s, global atmospheric temperature warming seemed to have slowed down (Trenberth & Fasullo, 2013). Previous work by England et al. (2014) indicates that ocean circulation change due to changes in momentum flux (wind stress) resulted in enhanced ocean heat uptake and the slowdown of the global atmospheric temperature warming in 2000s. Because of this, fluxes across the atmosphere-ocean interface are key to understanding historical and future changes in climate.

Ocean surface gravity waves (ocean waves hereafter) are ubiquitous across the world's oceans. Historically, the close covariation of waves with the ocean surface winds, by which they are forced, has typically led to waves being considered as a passive component in the atmosphere-ocean climate system. However, waves are not typically in equilibrium with the surface winds, with much of the energy of the wave field being contained in swell frequency bands (waves propagating faster than the winds; Hanley et al., 2010; Semedo et al., 2011). This disequilibrium can lead to ocean surface waves having a critical role in the atmosphere-ocean interaction. For example, momentum fluxes from atmosphere to ocean have been expressed as a function of wave state (Drennan et al., 2003; Janssen, 1991; Patton et al., 2019; Taylor & Yelland, 2001). The upper ocean structure is modified by turbulence in the surface ocean. Wave breaking injects a source of turbulence at the ocean surface (Craig & Banner, 1994), and wave-induced Langmuir cells are an additional source of turbulence capable of altering the surface ocean structure (McWilliams et al., 1997). This mixing alters the sea surface temperature, in-turn modifying the flux of heat across the atmosphere-ocean interface. Therefore, ocean wave conditions are an important consideration for estimating atmosphere-ocean fluxes.

Climate research on historical and future climate change has a strong dependence on climate simulations using Global Climate Models (GCMs). The atmosphere-ocean fluxes that have ocean wave dependence have generally been parameterized by surface winds only in GCMs, or ignored altogether. Observed historical changes in global ocean surface wind and wave climatology display different spatial patterns of change from each other (Young & Ribal, 2019). It follows that the assumed parameterizations of wave effects by wind might consequently be too simplified. Recently, impacts of ocean wave-dependent processes on GCM climate simulations have been studied. For example, wave-dependent momentum flux (Breivik et al., 2015; Chune & Aouf, 2018; Fan et al., 2012; Shimura et al., 2017), wave-dependent kinetic energy flux (Breivik et al., 2015), and wave-dependent upper ocean mixing by nonbreaking waves-induced turbulence (e.g., Qiao et al., 2016; Song et al., 2012; Stoney et al., 2018; Walsh et al., 2017) or wave-induced Langmuir turbulence (Fan & Griffies, 2014; Li et al., 2017) have been implemented into GCM, and the impacts have been explored. Wave impacts on heat flux imbalance at the atmosphere-ocean in the context of climate change, which is important as described above, have not been discussed in those previous studies. Here, we explore the impacts of ocean surface wave-dependent momentum flux on global ocean climate, especially heat flux imbalance at the atmosphere-ocean interface (ocean heat content change), using a global ocean model. Our results show the wave-dependent momentum flux can lead to significant modulation of ocean circulation, heat flux and the resultant ocean heat content which is key for understanding and projecting future and present climate change.

2. Methods

2.1. Global Ocean-Sea Ice Model

We conduct global ocean-sea ice climate simulations using the Modular Ocean Model version 5 (MOM5) (Griffies, 2012). The spatial resolution is set as 1° in longitude and 300 grids in latitudes, 0.25° to 1° depending on latitude, by tripolar grid coordination. The model has 50 vertical layers, with the upper 0–200 m discretized by 10 m intervals. The forcing data of MOM5 is derived from JRA-55 reanalysis (Kobayashi et al., 2015). Forcing data include 6-hourly 10 m height sea surface wind, surface temperature, humidity, sea level pressure, precipitation, shortwave radiation, longwave radiation, and climatology of river run off. The JRA-55 spatial resolution is approximately 60 km, which is interpolated onto the MOM5 grid spatially at a 2-hourly temporal resolution. The higher resolution global ocean models, such as 0.25° or 0.1° models, have been developed, and the impacts of resolution have been discussed by Kiss et al. (2020).

2.2. Ocean Surface Wave Data

Ocean surface wave data is not provided as part of the JRA-55 reanalysis. Wave data is produced independently using the WAVEWATCH III wave model (The WAVEWATCH III Development Group, 2016) forced with JRA-55's 6-hourly sea surface winds and monthly sea ice fraction. The source terms from Ardhuin et al. (2010) are used for input and dissipation terms. This data set was used to describe the wave climate by Shimura and Mori (2019) who presented good comparisons with buoy observations. Here, comparisons between global significant wave heights (H_s) from the JRA-55 forced wave hindcast and the altimeter observations of Ribal and Young (2019) are shown. The comparison period is 1992 to 2015 being the period with a

high number of altimeter observations. Supporting information Figure S1 presents the averaged H_s from the JRA-55 hindcast, and altimeter data sets. Consistent spatial patterns of H_s are seen between the two data sets. Figure S1b displays the bias between the JRA-55 forced hindcast and the altimeter data. The bias is up to 10% (0.5 m) in the Southern Ocean. In the Northern Hemisphere (NH), the JRA-55 forced hindcast overestimates H_s by up to 5% (0.3 m). On the other hand, H_s is underestimated by 10% (0.2 m) in the western equatorial Pacific. Overall, we conclude the JRA-55 wave hindcast provides an adequate representation of wave conditions to support the remainder of our study.

2.3. Momentum Flux Formulation

Typically, atmosphere or ocean models represent the momentum flux from atmosphere to ocean as follows:

$$\tau_{AO} = \rho_a u_*^2 = \rho_a C_m U^2 \quad (1)$$

where ρ_a is air density, u_* is the friction velocity in air, U is the 10 m height sea surface wind speed relative to ocean surface current, and C_m is the bulk transfer coefficient for momentum. Large and Yeager (2009) formulated the C_m depending on wind speed as follows:

$$C_m = 0.00270/U + 0.000142 + 0.0000764U - 3.14807 \times 10^{-13}U^6 \quad (U < 33\text{m/s}) \quad (2)$$

$$C_m = 0.00234 \quad (U \geq 33\text{m/s}) \quad (3)$$

Equations 1–3 mean that the momentum flux depends on just wind speed and surface currents. And the bulk transfer coefficient for heat (C_h) is formulated as

$$-u_* \theta_* = C_h U \Delta \theta, \quad (4)$$

$$C_h = 0.0180 \sqrt{C_m}; \quad \text{when stable} \quad (5)$$

$$C_h = 0.0327 \sqrt{C_m}; \quad \text{when unstable} \quad (6)$$

where θ_* is the temperature scale and $\Delta \theta$ is the difference in potential temperature between the air and sea surface. The formula of bulk transfer coefficient has been used commonly in global ocean-sea ice models (Griffies et al., 2014; Storto et al., 2016; Tsujino et al., 2018).

The formulation of Equations 1–3 ignore the influence of ocean waves. But in reality, almost all the momentum from the atmosphere goes to the waves at first, and then the ocean current receives the momentum from wave dissipation (Mitsuyasu, 1985).

The momentum flux to the ocean (τ_{ocn}) can be represented as a function of ocean waves as follows:

$$\tau_{ocn} = \rho_a u_*^2 - (\tau_{AW} - \tau_{WO}) \quad (7)$$

where τ_{AW} and τ_{WO} are the momentum flux from atmosphere to wave and wave to ocean current, respectively.

Spectral ocean wave models, such as WAVEWATCH III, solve the propagation of wave energy for each wave component in wave number (k) and direction (θ). The equation is described as

$$\frac{DF(k, \theta)}{Dt} = S(k, \theta) \quad (8)$$

where $F(k, \theta)$ is the wave energy spectrum, $\frac{D}{Dt}$ is the total derivative and S represents the sources and sinks of wave energy. In deep water, the S consists of three terms:

$$S(k, \theta) = S_{in}(k, \theta) + S_{ds}(k, \theta) + S_{nl}(k, \theta) \quad (9)$$

where S_{in} represents wind input, S_{ds} is wave dissipation, and S_{nl} are nonlinear wave-wave interaction terms. Integration of S_{in} and S_{ds} in spectral space can represent the τ_{AW} and τ_{WO} :

$$\tau_{AW} = \rho_w g \int \int \frac{S_{in}(k, \theta)}{c} dk d\theta \quad (10)$$

$$\tau_{WO} = \rho_w g \int \int \frac{S_{ds}(k, \theta)}{c} dk d\theta \quad (11)$$

where ρ_w is the water density, g is the gravitational acceleration, and c is wave phase speed. S_{in} and S_{ds} proposed by Ardhuin et al. (2010) are used in this study. u_* can be calculated at the same time of S_{in} because those variables are the implicit function of each other. S_{in} and S_{ds} are determined by sea surface wind speed and wave states. Therefore, u_* and τ_{ocn} are dependent on not only sea surface wind speed but also dependent on wave states.

2.4. Experimental Configuration

We conduct global ocean-sea ice climate simulations for the period 1958 to 2015. Two experiments are completed. The first experiment uses wind speed dependent momentum bulk transfer coefficient formulated in Equations 2 and 3. This is treated as a control experiment and denoted as “expWIND.” The second experiment formulates the momentum flux as a function of the JRA-55-derived wave hindcast, based on Equation 7. This experiment is denoted as “expWAVE.”

In the expWAVE, momentum flux to ocean τ_{ocn} is calculated using wave model outputs of u_* , τ_{AW} , and τ_{WO} . The expWAVE experiment implements the bulk transfer coefficient of heat formulated by Equations 5 and 6. Equations 5 and 6 require the C_m although C_m is not used in the calculation of τ_{ocn} . Thus, C_m in expWAVE is defined by the logarithm law below:

$$C_{m_{air}} = \left(\frac{\kappa}{\log\left(\frac{10}{z_{0m}}\right)} \right)^2 \quad (12)$$

where κ is the Karman constant. z_{0m} is the roughness by wave and determined by u_* of wave model output;

$$z_{0m} = \frac{10}{e^{\kappa U/u_*}} \quad (13)$$

To spin-up the ocean model, a 900 year simulation with repeated 1958 annual forcing is conducted for each experiment. The 58 year simulations for the period 1958 to 2015 are initialized with the state following the 900 year repeat simulation spin-up. We have control experiments for expWIND and expWAVE. Our analysis focuses on the last 30 years (1986 to 2015) of the simulation, being the period with greater observational record for comparison.

For comparison with C_m of expWIND with expWAVE, C_m of expWAVE is defined as

$$C_{m_{ocn}} = \frac{\tau_{ocn}}{\rho_a U^2} \quad (14)$$

3. Results and Discussion

3.1. Momentum Flux

The climatology of momentum flux in expWAVE is discussed here. Figure S2 is the ratio of differences in the climatology of τ_{ocn} and $\rho_a u_*^2$ calculated in expWAVE. The differences are small and range roughly from -2% to 0%. Negative value means that τ_{AW} is larger than τ_{WO} as explained by Equation 7. Larger negative values are seen in the middle to higher latitudes, particularly in the western part of the ocean basin in the NH. The western part of the North Pacific and Atlantic corresponds to the region where waves are in the initial stage of development. The differences are almost zero at lower latitudes.

Comparisons of momentum flux between expWIND and expWAVE show how the relationship between U_{10} and C_m is wave state dependent. Figure 1a shows the relationship between U_{10} and C_m . In Figure 1a, C_m is calculated by Equations 2 and 3 for expWIND and by Equation 14 for expWAVE using 30 years (1986–2015)

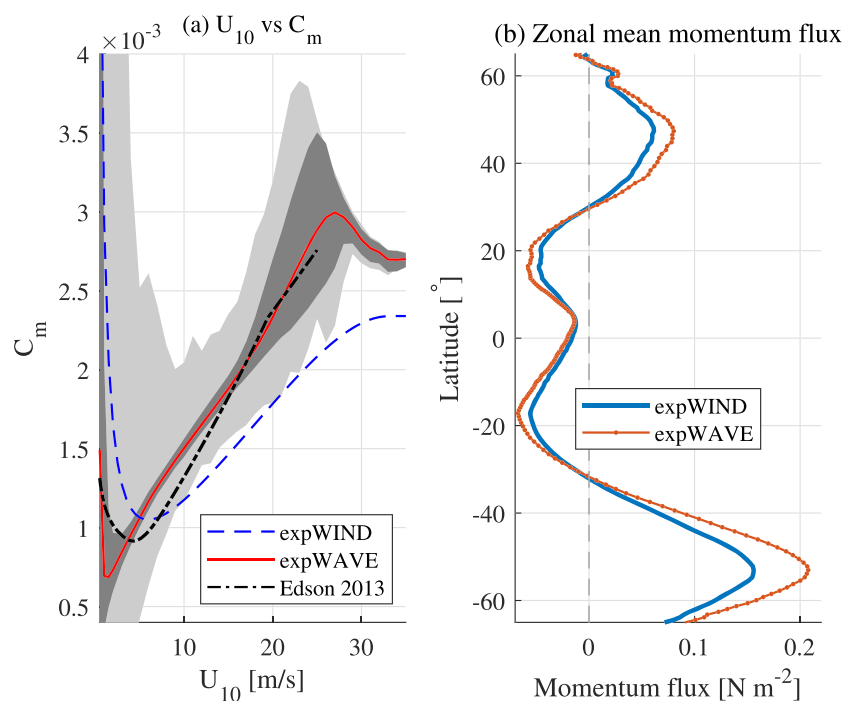


Figure 1. The comparison of momentum flux between expWAVE and expWIND. (a) The relationship between U_{10} and C_m . The red line, thick shade, and light shade indicate the mean value, 2 times of standard deviation, and minimum to maximum value. The black dash-dotted line is the formula of Edson et al. (2013). (b) Zonal mean zonal momentum flux climatology of expWIND and expWAVE.

of data from the Pacific region (50°S to 50°N, 175–179°W). In the expWIND, C_m corresponds uniquely with wind speed, as defined by Equation 2. In the expWAVE, C_m varies depending on the wave condition under a certain wind speed. The variation is greater for wind speed less than 5 m/s and for wind speeds greater than 15 m/s. The mean value of C_m in expWAVE is larger than that in expWIND when U_{10} is over 4 m/s. The differences in mean value of C_m between expWIND and expWAVE are about 0.0003 to 0.0005 when U_{10} is 10 to 20 m/s. The expWIND is placed at the lower limit of expWAVE when U_{10} is over 10 m/s. The expWAVE has a range of C_m consistent with observations (e.g., Figure 6 of Edson et al., 2013) although the results of flux observation are highly varied depending on individual studies. The formula proposed by Edson et al. (2013) is shown in Figure 1a as a reference. The momentum flux corresponding to U_{10} of expWAVE is larger than that of expWIND when U_{10} is over 10 m/s, same as C_m . The relationship between U_{10} and C_m as shown in Figure 1a doesn't depend on the spatial resolution. Therefore, it can be considered that the impacts of this relationship on the ocean climate as described below don't depend on spatial resolution.

Figure 1b presents the climatology (30 years averaged value) of zonal mean zonal (west-east direction) momentum flux for expWIND and expWAVE. Note that the positive (negative) values are eastward (westward) momentum flux. The momentum flux climatology of expWAVE is enhanced by 20% compared with expWIND for every latitude. The differences are about 0.02, 0.01, and 0.05 N/m⁻² for the NH midlatitudes, the trade wind regions, and the Southern Ocean, respectively.

3.2. Ocean Circulation Climatology

The differences in momentum flux between expWIND and expWAVE lead to differences in surface ocean circulation, represented using surface current and sea surface temperature (SST). The atmosphere to ocean momentum flux has direct influence on the ocean surface current. Figures 2a–2c show differences in climatology of the zonal ocean surface current. Figure 2b show the differences between expWAVE and expWIND (expWAVE - expWIND). The differences in current are larger in the equatorial current system. The

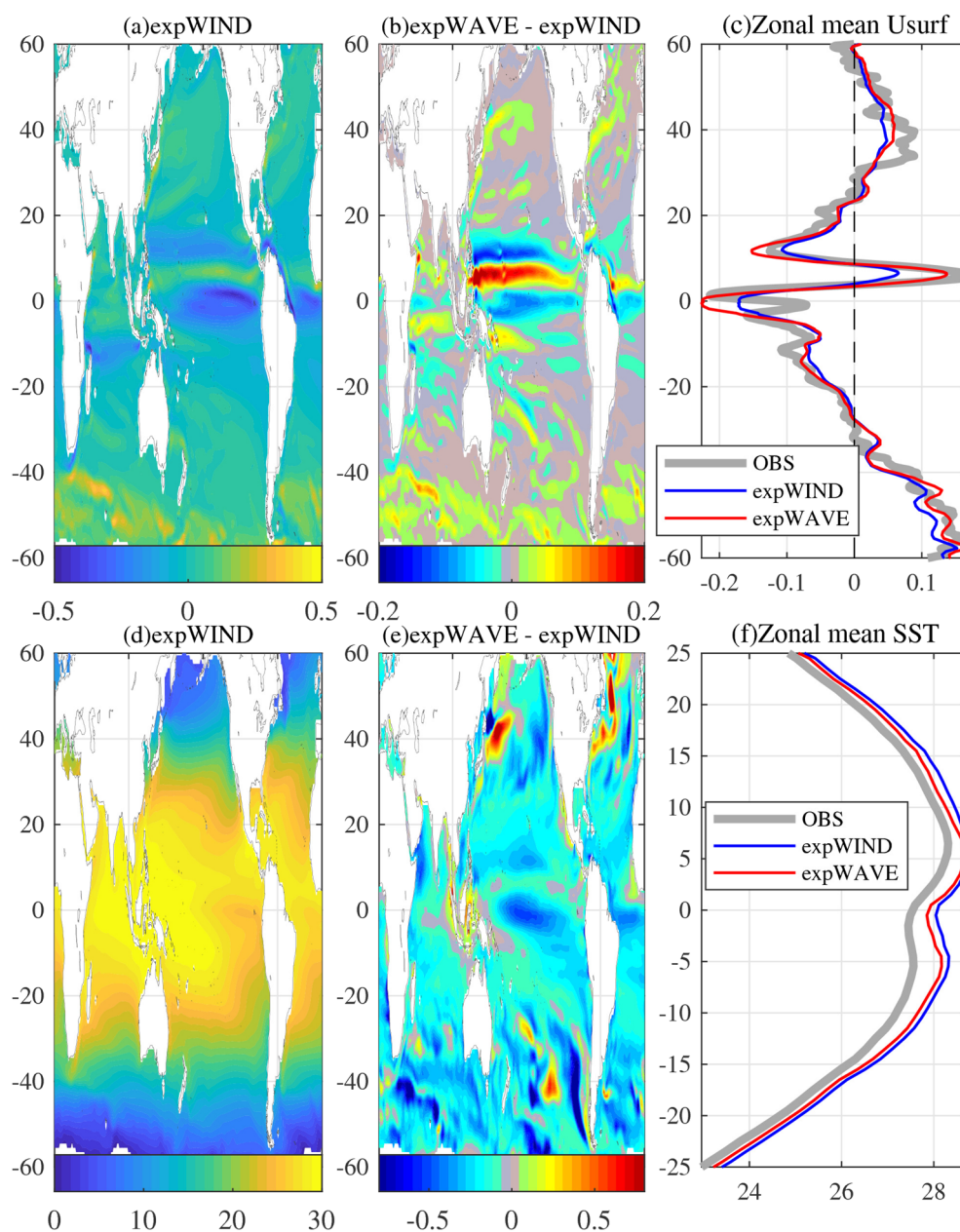


Figure 2. The climatology of ocean surface variables. (a) The climatology of the east-west component of surface current of expWIND (unit: ms^{-1}). (b) The differences between expWAVE and expWIND (expWAVE - expWIND). (c) Zonal mean value in comparison with observation. (d–f) Same as (a)–(c) but for SST (unit: $^{\circ}\text{C}$).

equatorial current system, including the westward current and the eastward counter current, is enhanced by 0.15 m/s in expWAVE compared with expWIND. In midlatitudes, the current is also enhanced in expWAVE although the enhancement in midlatitudes is less than seen in the equatorial regions. Figure 2c displays zonal mean zonal surface ocean current values for expWIND, expWAVE and observed drifter-derived climatology of global near-surface currents (Laurindo et al., 2017). It is clear that the surface current climatology from expWIND is much smaller than observed conditions all over the ocean. The expWAVE is nearer to the observational climatology than expWIND, with the zonal mean value of expWAVE larger than expWIND by about 30%. The meridional component of current leads to similar results to those described for the zonal flow (not shown).

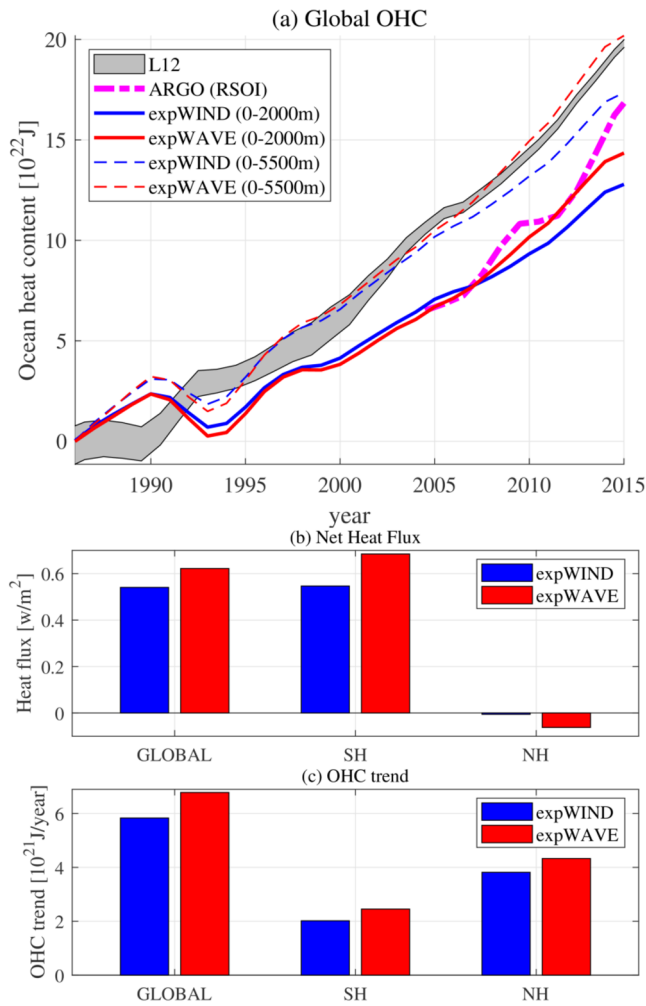


Figure 3. OHC change and net heat flux. (a) The 30 year time series of global OHC. The solid lines are for OHC in 0 to 2,000 m depth, and the broken lines are for OHC in full depth. The observation (ARGO) and objective analysis data (L12) are also plotted. Hemispheric contribution to (b) net heat flux and (c) trend of OHC in full depth. Global, SH, and NH values are plotted from left to right.

the 3 year moving averaged OHC anomaly is shown by subtracting the value of 1986. Both expWIND and expWAVE display a positive trend in OHC, however the increasing trend is larger in expWAVE than expWIND. The trends of OHC in 0 to 2,000 m depth during 1986 to 2015 are 4.2 and 4.7×10^{21} J/year for expWIND and expWAVE, respectively; the expWAVE trend being 12% greater than expWIND. The analysis data of Levitus et al. (2012) shows the trend of 7.1×10^{21} J/year. We find the trend taken from expWAVE better represents the objective analysis data, than that taken from expWIND. Looking at the OHC in full depth in the period 1986–2015 which correspond to the heat flux imbalance at the atmosphere-ocean, expWAVE shows an OHC trend 16% larger than expWIND; 6.8 and 5.8×10^{21} J/year respectively although we don't have an equivalent observed value. The globally covered ARGO period spans 2004 to 2015 only. Comparing trends over this period, we calculate trends in OHC of 10.1 , 8.8 , 5.9 and 8.1×10^{21} J/year for observation, analysis, expWIND and expWAVE, respectively. Here we see that expWAVE trends are significantly larger than expWIND trends (36%), and much closer to the observed trends.

OHC change corresponds to net heat flux at the ocean surface. Net heat flux was calculated as the sum of shortwave radiation, longwave radiation, sensible heat flux and latent heat flux. All heat fluxes, except the shortwave radiation, are sensitive to the surface flux parameterization used in expWIND and expWAVE,

Figures 2d–2f show the differences in SST climatology. The SST climatology in expWIND is lower than expWAVE by about 0.5°C globally. We explain this as a result of enhanced momentum flux in expWAVE driving a deeper mixed layer (Figure S3) and consequent lower upper temperature than expWIND. The magnitude of deepening is same order of Langmuir mixing shown by Li et al. (2019). At the equator, SST differences are larger than observed in other regions. This larger SST difference at the equator is the result of the strengthened surface current and increased up-welling in the expWAVE experiment. Figure 2f displays the difference between model experiment SST climatology and observations (HadISST; Rayner et al., 2003) for expWIND and expWAVE, respectively. Although both expWIND and expWAVE overestimate SST climatology, expWAVE shows the better representation of climatology compared with observation. Note that Figure 2f displays the region limited between 25°S and 25°N in order to make clear the differences. Similar tendencies are seen at higher latitudes.

3.3. Ocean Heat Content Change

Ocean heat content change is a key metric of climate change, closely linked to global atmospheric temperature change, and also defines the thermosteric component of sea level rise. Global ocean heat content (OHC) is calculated as follows:

$$OHC = \int_z \int_A c_p \rho T dz da \quad (15)$$

where c_p is heat capacity, T is potential temperature and a is surface area. The OHC of control experiments were subtracted from that of expWIND and expWAVE to remove the drift following Gupta et al. (2013). Even if this subtraction of control experiment value is not applied, the results are almost same. This suggest that the model reaches close to quasi-steady state at the end of the 900 year spin-up simulation.

Figure 3a displays the 30 year (1986–2015) time series of global OHC in 0 to 2,000 m depth as well as full depth (0 to 5,500 m). Observed and objective analysis data are also shown as references. The observed data shown are ARGO observations taken from Roemmich et al. (2015). The objective analysis data is taken from Levitus et al. (2012). Note that the observation and analysis data are based on the OHC from 0 to 2,000 m. In the figure,

despite the atmospheric forcing being the same. Consistent with *OHC*, heat fluxes of control experiments were subtracted from those of expWAVE and expWIND. Net heat fluxes of the expWIND and expWAVE during 1986 to 2015 (2004 to 2015) are 0.54 (0.70) and 0.62 (0.93) W/m^2 , respectively, and thus the net heat flux of expWAVE is larger by 15% (33%) than expWIND. This is consistent with the full depth *OHC* trend; expWAVE is larger by 16% than expWIND. Note that net heat flux is estimated as 10 to 15 W/m^2 based on satellite-based products during 2006 to 2015 and the uncertainty is quite large currently as $\pm 15 \text{ W/m}^2$ (Meyssignac et al., 2019). Figure 3b shows the contribution of each hemisphere to global net heat flux. The areal sum of heat flux is divided by the global ocean area, instead of each hemisphere ocean area; that is, the sum of SH and NH heat flux equals the global heat flux. From this it is clear that heat flux to the ocean in SH is much larger than that in NH. This is consistent with the findings of Irving et al. (2019) based on analysis of historical simulations from CMIP5. Furthermore, the differences in global ocean heat flux between the expWIND and expWAVE can be largely attributed to the SH differences. Figure 3c shows the contribution of each hemisphere to global full depth *OHC*. *OHC* in NH shows a stronger trend than that in SH for both experiments, and the expWAVE shows the larger trend for both hemispheres than expWIND. The hemispheric gradient of heat flux of expWAVE is larger than expWIND while that of *OHC* trend is similar between experiments, which implies a stronger northward heat transport in expWAVE. This can be because of the stronger circulation seen in expWAVE relative to expWIND. Figure S4 shows the Meridional Overturning Circulation (MOC) for expWIND, expWAVE, and the difference. It is clear that MOC of expWAVE is stronger than expWIND, especially around 1,000 m depth which is dominated by Atlantic MOC (AMOC). The observation of McCarthy et al. (2015) estimated the AMOC at 26° as 17.2 Sv. The AMOC at 26° of expWIND and expWAVE are 7.7 and 11.2 Sv, indicating expWAVE represents observed AMOC more closely than expWIND. The stronger MOC of expWAVE can lead to stronger northward heat transport. If looking at the period 2006 to 2015, both heat flux and trend of *OHC* in SH is much larger than those of NH which is consistent with previous studies (Rathore et al., 2020; Roemmich et al., 2015), and the heat flux in SH by expWAVE is larger by 0.24 W/m^2 than expWIND which dominates the global heat flux difference same as the period 1986 to 2015 (Figure 3b).

4. Conclusions

Atmosphere-ocean flux is a key factor to understand the dynamics of the Earth system. To date the role of ocean surface waves are often overlooked in current ocean models, despite the influence of ocean surface wave state on atmosphere-ocean flux. This study explored the impacts of ocean surface waves-dependent momentum flux on the global ocean climatology, using a global ocean-sea ice model. The ocean-sea ice model, MOM5, was forced using the atmospheric conditions taken from the JRA-55 reanalysis, with addition of wave conditions derived from a JRA-55 forced wave hindcast spanning the period 1958 to 2015. Two ocean climate experiments, with and without the influence of waves, were compared with each other.

In comparisons of simulated sea surface variables, including surface current and SST, with the observations, we show that ocean climate simulations forced with wave-dependent momentum fluxes can represent the climatology better than that forced by wind only dependent momentum fluxes. We see that these differences lead to the ocean heat flux and *OHC* differences. The trend in *OHC* over the past 30 years is estimated to be 16% larger in expWAVE than expWIND; The larger trend seen in the expWAVE is nearer to observed trends. The larger increase in *OHC* of expWAVE, relative to expWIND, can be attributed to the increase in net heat flux of the SH. We note here that the greatest changes in wave heights in the historical record occur in the Southern Ocean (Young & Ribal, 2019), and furthermore, it is the waves of the Southern Ocean which appear most sensitive to future climate scenarios (Morim et al., 2019). On the other hand the larger increase in *OHC* of expWAVE in the NH than expWIND can be attributed to the stronger MOC. AMOC can control CO_2 flux into ocean (Pérez et al., 2013). Therefore, it can be speculated that the differences between expWIND and expWAVE have significant impacts on climate change projection via CO_2 concentration differences.

Here, the difference in *OHC* change between expWIND and expWAVE is compared with intermodel variance among CMIP5 climate models. CMIP5 climate models were used for climate change impact assessment in IPCC-AR5 (Flato et al., 2013). The CMIP5 climate model *OHC* data compiled by Cheng et al. (2019) is used (<https://159.226.119.60/cheng/>). The mean trend and standard deviation of 0 to 2,000 m *OHC* in 33 models during 1986 to 2015 (2004 to 2015) is 8.8 ± 2.3 (10.7 ± 2.2) $\times 10^{21} \text{ J/year}$. The differences between

expWIND and expWAVE are $0.5(2.2) \times 10^{21}$ J/year, which correspond to 22% (100%) of standard deviation of CMIP5. The difference is not large compared with the intermodel variance of CMIP5 but is not negligible.

Previous studies using wave-coupled GCM, in terms of the impacts on ocean climate, have focused mainly on SST or upper ocean temperature (e.g., 0–300 m) (Breivik et al., 2015; Chune & Aouf, 2018; Stoney et al., 2018; Walsh et al., 2017) and mixed layer depth (Li et al., 2017; Qiao et al., 2016; Song et al., 2012). Net heat flux and the resultant *OHC* change, important metrics for monitoring the state of the climate, have not been discussed. Breivik et al. (2015) and Stoney et al. (2018) analyzed just upper ocean heat content in 0 to 300 m. In order to estimate *OHC* change that takes account of the deep ocean from an ocean model requires long-term spin up simulations to be completed, to account for model drift. The 900 year spin up enables this study to estimate the net heat flux and *OHC* change. Therefore, we consider that this study provides new insight into the impact of wave-dependent process on climate.

This study focused only on the ocean wave modulated momentum flux although there are other wave-dependent processes that should be taken into account (Cavaleri et al., 2012). Coupling between atmosphere and waves has significant impacts on the atmospheric circulation location, such as storm belt at the midlatitudes and the Hadley circulation, in addition to magnitude of surface wind speed (Janssen & Viterbo, 1996; Shimura et al., 2017). Therefore, coupling between atmosphere-ocean-waves may change ocean gyre location to some extent. Contributions of each wave-dependent process in the climate system should be estimated and the high impact processes need to be implemented into operational climate models as we seek to develop seamless Earth System Prediction systems (Ruti et al., 2019). Although this study focuses on the ocean climate for the historical period, it can be considered that wave-dependent momentum flux can have nonnegligible impacts on future climate projections because of the significant differences in trend among the experiments. Despite the future tasks described above, we conclude that ocean climate simulations using a wave-dependent momentum flux parameterization can alter the ocean climatology and trend representation by more than 15%. Changes of this magnitude are not negligible in the context of climate change estimations.

Data Availability Statement

Ocean climate simulation data can be available in the repository of ZENODO (<https://doi.org/10.5281/zenodo.3886853>).

References

- Arduhin, F., Rogers, E., Babanin, A. V., Filipot, J.-F., Magne, R., Roland, A., et al. (2010). Semiempirical dissipation source functions for ocean waves. Part I: Definition, calibration, and validation. *Journal of Physical Oceanography*, *40*(9), 1917–1941.
- Balmaseda, M. A., Trenberth, K. E., & Källén, E. (2013). Distinctive climate signals in reanalysis of global ocean heat content. *Geophysical Research Letters*, *40*, 1754–1759. <https://doi.org/10.1002/grl.50382>
- Breivik, O., Mogenssen, K., Bidlot, J.-R., Balmaseda, M. A., & Janssen, P. A. E. M. (2015). Surface wave effects in the NEMO ocean model: Forced and coupled experiments. *Journal of Geophysical Research: Oceans*, *120*, 2973–2992. <https://doi.org/10.1002/2014JC010565>
- Cavaleri, L., Fox-Kemper, B., & Hemer, M. (2012). Wind waves in the coupled climate system. *Bulletin of the American Meteorological Society*, *93*(11), 1651–1661.
- Cheng, L., Abraham, J., Hausfather, Z., & Trenberth, K. E. (2019). How fast are the oceans warming? *Science*, *363*(6423), 128–129.
- Chune, S. L., & Aouf, L. (2018). Wave effects in global ocean modeling: Parametrizations vs. forcing from a wave model. *Ocean Dynamics*, *68*(12), 1739–1758.
- Craig, P. D., & Banner, M. L. (1994). Modeling wave-enhanced turbulence in the ocean surface layer. *Journal of Physical Oceanography*, *24*(12), 2546–2559.
- Drennan, W. M., Graber, H. C., Hauser, D., & Quentin, C. (2003). On the wave age dependence of wind stress over pure wind seas. *Journal of Geophysical Research*, *108*(C3), 8062. <https://doi.org/10.1029/2000JC000715>
- Edson, J. B., Jampana, V., Weller, R. A., Bigorre, S. P., Plueddemann, A. J., Fairall, C. W., et al. (2013). On the exchange of momentum over the open ocean. *Journal of Physical Oceanography*, *43*(8), 1589–1610.
- England, M. H., McGregor, S., Spence, P., Meehl, G. A., Timmermann, A., Cai, W., et al. (2014). Recent intensification of wind-driven circulation in the Pacific and the ongoing warming hiatus. *Nature Climate Change*, *4*(3), 222.
- Fan, Y., & Griffies, S. M. (2014). Impacts of parameterized Langmuir turbulence and nonbreaking wave mixing in global climate simulations. *Journal of Climate*, *27*(12), 4752–4775.
- Fan, Y., Lin, S.-J., Held, I. M., Yu, Z., & Tolman, H. L. (2012). Global ocean surface wave simulation using a coupled atmosphere-wave model. *Journal of Climate*, *25*(18), 6233–6252.
- Flato, G., Marotzke, J., Abiodun, B., Braconnot, P., Chou, S. C., Collins, W., et al. (2013). Evaluation of climate models. In *Climate change 2013: The physical science basis. Contribution of Working Group I to the Fifth Assessment Report of the Intergovernmental Panel on Climate Change* (pp. 741–866). Cambridge, UK and New York, NY: Cambridge University Press.
- Griffies, S. M. (2012). Elements of the modular ocean model (MOM). *GFDL Ocean Group Tech. Rep.*, *7*, 620.

Acknowledgments

T. S. was supported by JSPS KAKENHI Grant Numbers 19K15099, 18H03791, and 19H00782. This research was supported under the Integrated Research Program for Advancing Climate Models (TOUGOU) Grant Number JPMXD0717935498 by the Ministry of Education, Culture, Sports, Science, and Technology (MEXT). M. H. is supported by the Australian Commonwealth National Environmental Science Program Earth Systems and Climate Change Hub.

- Griffies, S. M., Yin, J., Durack, P. J., Goddard, P., Bates, S. C., Behrens, E., et al. (2014). An assessment of global and regional sea level for years 1993–2007 in a suite of interannual CORE-II simulations. *Ocean Modelling*, *78*, 35–89.
- Gupta, A. S., Jourdain, N. C., Brown, J. N., & Monselesan, D. (2013). Climate drift in the CMIP5 models. *Journal of Climate*, *26*(21), 8597–8615.
- Hanley, K. E., Belcher, S. E., & Sullivan, P. P. (2010). A global climatology of wind–wave interaction. *Journal of Physical Oceanography*, *40*(6), 1263–1282.
- Irving, D. B., Wijffels, S., & Church, J. A. (2019). Anthropogenic aerosols, greenhouse gases, and the uptake, transport, and storage of excess heat in the climate system. *Geophysical Research Letters*, *44*(6), 4894–4903. <https://doi.org/10.1029/2019GL082015>
- Janssen, P. A. E. M. (1991). Quasi-linear theory of wind-wave generation applied to wave forecasting. *Journal of Physical Oceanography*, *21*(11), 1631–1642.
- Janssen, P. A. E. M., & Viterbo, P. (1996). Ocean waves and the atmospheric climate. *Journal of Climate*, *9*(6), 1269–1287.
- Kiss, A. E., Hogg, A. M., Hannah, N., Boeira Dias, F., Brassington, G. B., Chamberlain, M. A., et al. (2020). ACCESS-OM2 v1.0: A global ocean-sea ice model at three resolutions. *Geoscientific Model Development*, *13*(2), 401–442.
- Kobayashi, S., Ota, Y., Harada, Y., Ebata, A., Moriya, M., Onoda, H., et al. (2015). The JRA-55 reanalysis: General specifications and basic characteristics. *Journal of the Meteorological Society of Japan. Ser. II*, *93*(1), 5–48.
- Large, W. G., & Yeager, S. G. (2009). The global climatology of an interannually varying air–sea flux data set. *Climate Dynamics*, *33*(2–3), 341–364.
- Laurindo, L. C., Mariano, A. J., & Lumpkin, R. (2017). An improved near-surface velocity climatology for the global ocean from drifter observations. *Deep Sea Research Part I: Oceanographic Research Papers*, *124*, 73–92.
- Levitus, S., Antonov, J. I., Boyer, T. P., Baranova, O. K., Garcia, H. E., Locarnini, R. A., et al. (2012). World ocean heat content and thermohaline sea level change (0–2000 m), 1955–2010. *Geophysical Research Letters*, *39*, L10603. <https://doi.org/10.1029/2012GL051106>
- Li, Q., Fox-Kemper, B., Breivik, O., & Webb, A. (2017). Statistical models of global Langmuir mixing. *Ocean Modelling*, *113*, 95–114.
- Li, Q., Reichl, B. G., Fox-Kemper, B., Adcroft, A. J., Belcher, S. E., Danabasoglu, G., et al. (2019). Comparing ocean surface boundary vertical mixing schemes including Langmuir turbulence. *Journal of Advances in Modeling Earth Systems*, *11*, 3545–3592. <https://doi.org/10.1029/2019MS001810>
- McCarthy, G. D., Smeed, D. A., Johns, W. E., Frajka-Williams, E., Moat, B. I., Rayner, D., et al. (2015). Measuring the Atlantic Meridional Overturning Circulation at 26N. *Progress in Oceanography*, *130*, 91–111.
- McWilliams, J. C., Sullivan, P. P., & Moeng, C.-H. (1997). Langmuir turbulence in the ocean. *Journal of Fluid Mechanics*, *334*, 1–30.
- Meehl, G. A., Arblaster, J. M., Fasullo, J. T., Hu, A., & Trenberth, K. E. (2011). Model-based evidence of deep-ocean heat uptake during surface-temperature hiatus periods. *Nature Climate Change*, *1*(7), 360.
- Meyssignac, B., Boyer, T., Zhao, Z., Hakuba, M. Z., Landerer, F. W., Stammer, D., et al. (2019). Measuring global ocean heat content to estimate the Earth energy imbalance. *Frontiers in Marine Science*, *6*, 432. <https://doi.org/10.3389/fmars.2019.00432>
- Mitsuyasu, H. (1985). A note on the momentum transfer from wind to waves. *Journal of Geophysical Research*, *90*(C2), 3343–3345.
- Morim, J., Hemer, M., Wang, X. L., Cartwright, N., Trenham, C., Semedo, A., et al. (2019). Robustness and uncertainties in global multi-variate wind-wave climate projections. *Nature Climate Change*, *9*(9), 711–718. <https://doi.org/10.1038/s41558-019-0542-5>
- Patton, E. G., Sullivan, P. P., Kosović, B., Dudhia, J., Mahrt, L., Žagar, M., & Marić, T. (2019). On the influence of swell propagation angle on surface drag. *Journal of Applied Meteorology and Climatology*, *58*(5), 1039–1059. <https://doi.org/10.1175/jamc-d-18-0211.1>
- Pérez, F. F., Mercier, H., Vázquez-Rodríguez, M., Lherminier, P., Velo, A., Pardo, P. C., et al. (2013). Atlantic ocean CO₂ uptake reduced by weakening of the meridional overturning circulation. *Nature Geoscience*, *6*(2), 146.
- Qiao, F., Yuan, Y., Deng, J., Dai, D., & Song, Z. (2016). Wave–turbulence interaction-induced vertical mixing and its effects in ocean and climate models. *Philosophical Transactions of the Royal Society A: Mathematical, Physical and Engineering Sciences*, *374*(2065), 20150201.
- Rathore, S., Bindoff, N. L., Phillips, H. E., & Feng, M. (2020). Recent hemispheric asymmetry in global ocean warming induced by climate change and internal variability. *Nature Communications*, *11*(1), 1–8.
- Rayner, N. A., Parker, D. E., Horton, E. B., Folland, C. K., Alexander, L. V., Rowell, D. P., et al. (2003). Global analyses of sea surface temperature, sea ice, and night marine air temperature since the late nineteenth century. *Journal of Geophysical Research*, *108*(D14), 4407. <https://doi.org/10.1029/2002JD002670>
- Rhein, M., Rintoul, S. R., Aoki, S., Campos, E., Chambers, D., Feely, R. A., et al. (2013). Observations: Ocean. In *Climate change 2013: The physical science basis. Contribution of Working Group I to the Fifth Assessment Report of the Intergovernmental Panel on Climate Change* (pp. 255–315). Cambridge, United Kingdom and New York, NY, USA: Cambridge University Press.
- Ribal, A., & Young, I. R. (2019). 33 years of globally calibrated wave height and wind speed data based on altimeter observations. *Scientific Data*, *6*, 77.
- Roemmich, D., Church, J., Gilson, J., Monselesan, D., Sutton, P., & Wijffels, S. (2015). Unabated planetary warming and its ocean structure since 2006. *Nature Climate Change*, *5*(3), 240.
- Ruti, P., Tarasova, O., Keller, J., Carmichael, G., Hov, O., Jones, S., et al. (2019). Advancing research for seamless Earth system prediction. *Bulletin of the American Meteorological Society*, *101*(1), E23–E35.
- Semedo, A., Sušelj, K., Rutgersson, A., & Sterl, A. (2011). A global view on the wind sea and swell climate and variability from ERA-40. *Journal of Climate*, *24*(5), 1461–1479.
- Shimura, T., & Mori, N. (2019). High-resolution wave climate hindcast around Japan and its spectral representation. *Coastal Engineering*, *151*, 1–9. <https://doi.org/10.1016/j.coastaleng.2019.04.013>
- Shimura, T., Mori, N., Takemi, T., & Mizuta, R. (2017). Long-term impacts of ocean wave-dependent roughness on global climate systems. *Journal of Geophysical Research: Oceans*, *122*, 1995–2011. <https://doi.org/10.1002/2016JC012621>
- Song, Z., Qiao, F., & Song, Y. (2012). Response of the equatorial basin-wide SST to non-breaking surface wave-induced mixing in a climate model: An amendment to tropical bias. *Journal of Geophysical Research*, *117*, C00J26. <https://doi.org/10.1029/2012JC007931>
- Stoney, L., Walsh, K. J. E., Thomas, S., Spence, P., & Babanin, A. V. (2018). Changes in ocean heat content caused by wave-induced mixing in a high-resolution ocean model. *Journal of Physical Oceanography*, *48*(5), 1139–1150.
- Storto, A., Yang, C., & Masina, S. (2016). Sensitivity of global ocean heat content from reanalyses to the atmospheric reanalysis forcing: A comparative study. *Geophysical Research Letters*, *43*, 5261–5270. <https://doi.org/10.1002/2016GL068605>
- Taylor, P. K., & Yelland, M. J. (2001). The dependence of sea surface roughness on the height and steepness of the waves. *Journal of Physical Oceanography*, *31*(2), 572–590.
- The WAVEWATCH III Development Group (2016). User manual and system documentation of WAVEWATCH III Version 5.16.
- Trenberth, K. E., & Fasullo, J. T. (2013). An apparent hiatus in global warming? *Earth's Future*, *1*, 19–32. <https://doi.org/10.1002/2013EF000165>

- Tsujino, H., Urakawa, S., Nakano, H., Small, R. J., Kim, W. M., Yeager, S. G., et al. (2018). JRA-55 based surface dataset for driving ocean–sea-ice models (JRA55-do). *Ocean Modelling*, *130*, 79–139.
- Walsh, K., Govekar, P., Babanin, A. V., Ghantous, M., Spence, P., & Scoccimarro, E. (2017). The effect on simulated ocean climate of a parameterization of unbroken wave-induced mixing incorporated into the k-epsilon mixing scheme. *Journal of Advances in Modeling Earth Systems*, *9*, 735–758. <https://doi.org/10.1002/2016MS000707>
- Young, I. R., & Ribal, A. (2019). Multiplatform evaluation of global trends in wind speed and wave height. *Science*, *364*, 548–552.